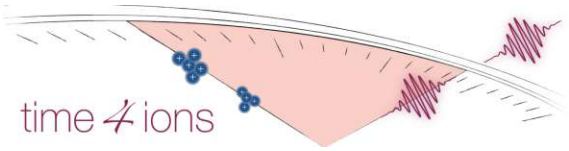

DIPLOMARBEIT

Energy and charge transfer of light ions transmitted through free-standing 2D materials

Zur Erlangung des akademischen Grades

Diplom-Ingenieur

im Rahmen des Studiums

Technische Physik

eingereicht von

Lukas Fischer
Matrikelnummer 0132537

Ausgeführt am

Institut für Angewandte Physik
der Fakultät für Physik
der Technischen Universität Wien

Unter Anleitung von

Dipl.Ing. Anna NIGGAS
Assoc.Prof. Dr. Richard A. WILHELM

Wien, April 29, 2024

Lukas Fischer

Richard A. Wilhelm

Abstract

There are still open questions in understanding the stopping of slow ions in 2D materials, since common descriptions for bulk materials cannot be directly adopted for the thin film limit. This work focuses on the energy and charge transfer of light, singly charged ions transmitted through 2D materials, setting up a comparatively simple system in contrast to multiply charged heavy ions. This enables a comparison to theoretical models, such as time-dependent density-functional theory (TD-DFT) calculations. In particular in our experiment we use 1-5 keV H^+ and He^+ and study their interaction with free-standing single-layer graphene and monolayer MoS_2. The energy of transmitted particles is measured charge-state dependent, using an electrostatic analyser for charged and a time of flight approach for neutralised particles. We observe a linear increase of energy transfer with ion velocity, in good agreement with TD-DFT. Additionally, we note a higher energy transfer for ions capturing an electron.

Kurzfassung

Die Wechselwirkung von langsamen Ionen in 2D Materialien ist noch Gegenstand aktueller Forschung, da übliche Beschreibungen für diese Wechselwirkungen mit makroskopischen Festkörpern nicht im Regime der dünnen Schichten übernommen werden kann. Diese Arbeit konzentriert sich auf den Energie- und Ladungsaustausch von leichten, einfach geladenen Ionen während des Durchdringens von 2D Materialien. Dieses vergleichsweise einfache System ist ideal zur Untersuchung und dem Vergleich zu zeitabhängiger Dichtefunktionaltheorie Simulationen (TD-DFT), um in weiterer Folge auf komplexere Systeme wie hochgeladene Ionen zurückschließen zu können. In den hier beschriebenen Versuchen werden konkret Wasserstoff und Helium ionisiert und mit 1-5 keV beschleunigt, um die Wechselwirkung mit einer frei stehenden atomaren Schicht von Graphen und MoS_2 zu untersuchen. Die Energie der Teilchen nach dem Durchdringen des 2D Materials wird ladungsabhängig gemessen. Für Ionen, die nach Transmission noch immer geladen sind, wird ein elektrostatischer Analysator verwendet und der Energieverlust von vollständig neutralisierte Teilchen wird mit einer Flugzeitmessung bestimmt. Wir beobachten eine lineare Abhängigkeit des Energietransfers von der Ionengeschwindigkeit, in guter Übereinstimmung mit TD-DFT Simulationen. Zusätzlich können wir einen höheren Energietransfer für Ionen, die durch den Einfang eines Elektrons neutralisiert werden, feststellen.

Contents

1. Introduction

In the first of this chapter a brief overview of the interaction between ions and bulk solids is presented. Since these findings can differ when delving into the regime of thin film and monoatomar layers, which are in focus of this work, in the second part 2D materials are discussed. Finally, motivations as to why an expansion into this regime is desirable and how this work is trying to approach this challenge.

1.1. Fundamentals of ion-solid interaction

When a charged particle approaches and subsequently impacts and passes through a material, a wide range of processes and phenomena might manifest when interacting with the electronic and nuclear system of the material. These include but are not limited to the emission of secondary particles (electrons, photons or atoms of the target material), the implantation or backscattering of the ion, or deformation of the crystal structure of a target. To understand the origin of these processes and the consequences of different combination of projectile and target, precise knowledge of the scattering events of the ion with the nuclear and electronic system of the target is required.

Whereas in the past, experiments were limited to α particles produced from radioactive substances [1], following the technological advancement in the construction of ion sources and accelerators, it now possible to produce a wide variety of ions, tuneable in ion masses, charge states, and kinetic energies. The possibility to select ion species with tailored properties for different use cases, lead for ions to be a popular tool for different application, ranging from analysis techniques [2, 3], to manufacturing and modification processes [4, 5] and for them to be even promising for applications in medicine [6].

Key to fully utilise many of the mentioned techniques is precise knowledge of how and where the energy of the ion is transferred to the target material and in what way the energy then dissipates. A first approach is to introduce a stopping force B, defined as transferred energy dE from the ion to the sample per unit length dx:

$$B = -\frac{dE}{dx} \tag{1.1}$$

A more universal quantity is the stopping cross section, as it describes the stopping power per target atom:

$$\frac{B}{\rho} = S = S_e + S_n, \tag{1.2}$$

with ρ the atomic density of the target. The stopping cross section S can further be separated into nuclear S_n and electronic S_e contributions, which can be beneficial, as the different contributions usually describe the stopping of ion with low and high energies respectively.

Beside the transfer of energy, the behaviour of charge is another important part in the description of the interaction. For an ion moving inside a material with a given velocity, a competition between neutralisation and further ionising processes leads for the traversing ion to reach an equilibrium charge state Z_{eff}. As the cross section of these processes is dependent on the velocity of said ion, so is its mean equilibrium charge state, which can be described by the following:

$$Z_{eff} = Z(1 - \exp^{-\frac{v}{v_0}Z^{-\frac{2}{3}}}) \tag{1.3}$$

with Z being the atomic number of an ion that moves with velocity v and v_0 being the Bohr velocity. The ratio $\frac{v}{v_0}$ points to the assumption, that only ions moving slower than electrons in typical orbit, can be bonded with.

A tried description of the energy dissipation of ions in the regime of low velocity electronic energy loss is the model established by Lindhard and Scharff in 1964 [7]. It considers screening effects of the atomic potentials and describes the scattering potential as the geometrical mean of the atomic potentials of target and projectile, yielding an electronic stopping cross section of

$$S_e = \frac{8\pi e^2 a_0}{4\pi\epsilon_0} \frac{Z_1^{7/6} Z_2}{\left(Z_1^{2/3} + Z_2^{2/3}\right)^{3/2}} \frac{v}{v_0}, \tag{1.4}$$

with e being the elementary charge, a_0 the Bohr radius, ϵ_0 the vacuum electric permittivity and Z_1 and Z_2 the atomic number of ion and target atoms respectively. Note, that for $Z_1 = Z_2 = Z$ follows that $S_e \propto v\, Z^{7/6}$. Furthermore, the energy transfer depends on the scattering angle i.e. the ion trajectory. This complicates the comparison of theoretical results, that usually consider integrated stopping S_e, to experimental data, where only the energy loss dE in a small angle can be measured due to finite detector size [8]. By now there are many first-principle calculations ranging from binary collision approximation for stopping as implemented in SRIM [11], to perturbation treatments [9] and density functional theories [10] to state-of-the-art code packages in the Ehrenfest regime as GPAW [12].

1.2. 2D materials

Since the first successful isolation and characterisation of a sheet of graphene, exfoliated from graphite [13], a new class of materials has been discovered and simultaneously a new field of research has been born.

Graphene is a planar monolayer of carbon atoms in a honeycomb lattice (figure 1.1a) and since the spacial extension of this sheet is restricted in one dimension to the width of just one atom, it is coined a 2D material. Despite the geometric constraints of graphene and other 2D materials, the diversity of their physical properties are as vast as novel, resulting in a fast popularity of this material class in the scientific community [14].

Graphene is not only an outstanding conductor with high carrier mobility [15] and density [16] at room-temperature, but an even bigger reason for interest in graphene is its unique electronic structure [17, 18]. It exhibits a quasi linear dispersion, allowing the effective description of electronic transport with massless Dirac fermion quasiparticles; with Dirac points, the crossing of conduction and valence band, pinned to the fermi

level [18, 19, 20]. Additionally, when stacking two layers of graphene on top of each other and then rotating the layers to a so-called "magic-angle", the system starts to exhibit superconductivity [21]. Beside the fascinating electronic system in graphene, its predicted mechanical properties ranging form an immense breaking strength [22] to high elasticity [23], and its even excellent reported thermal conductivity [24] while being atomically flat, opens a broad field of research and possible applications.

There are also other groups of 2D materials, like transition-metal dichalcogenides (TMDC). They are layered semiconductors obeying the chemical formal MX_2, with M being a transition-metal and X a chalcogen. A prominent example of this material class is MoS_2, as depicted in figure 1.1b. Even if it consists of actually three layers, it is still considered a 2D material, due to its extraordinary thinness as well as strong in-plane and weak out-of-plane bonding, allowing it to be fabricated like graphene from exfoliation [17]. It is a semi-conductor with the band gap changing from a 1.3 eV indirect band gap in the bulk to a 1.8 eV direct band gap in its 2D form [26].

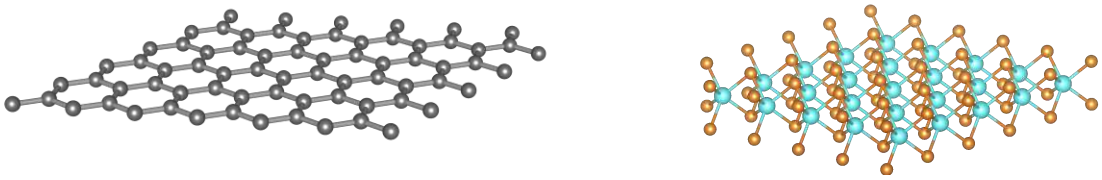

(a) SLG (b) MoS_2

Figure 1.1.: Rendered images of (a) free-standing single-layer graphene (SLG) and (b) monolayer MoS_2. Renders were done using the free software VESTA [25].)

While the two materials highlighted in this section are worthy of being researched on their own, there are attempts to combine these layer into van der Waals heterostructures in an attempt to utilise the most promising aspects of both materials in a single device, especially in optoelectronics [27, 28].

1.3. Motivation

Many of the considerations made in section 1.1, assume and rely on a target with finite thickness. While this is a given for most material classes, this assumption starts to fail in the limit of monoatomic layers of exotic 2D materials. For example, in a 2D material an equilibrium state cannot be achieved during transmission and scattering is limited to a smaller amount of collision events, leading to more forward scattering. Even if the description fails for bulk materials, the investigation of the evolution of energy and charge transfer can still be of great interest, as their observation grants insight into the microscopic processes.

To further harness the potential of 2D materials and their heterostructures, new ways to modify, structure and benchmark them are desired. A promising tool for that purpose, investigated here at TU Wien, are highly charged ions [29, 30, 31, 32, 33] as their high potential energy and relatively low kinetic energy allow a unique way of interaction of

ions with matter, depositing their energy very fast in close vicinity of the impact point [34, 35, 36].

These exotic materials and tools require new approaches, both computational and experimental. Current state-of-the-art TD-DFT simulations in the Ehrenfest regime are done by collaborators at Helmholtz-Zentrum Dresden-Rossendorf on the 2D materials introduced in 1.2, and can in principle describe the physics of the energy and charge dynamics of highly charged ions interacting with matter. Ehrenfest dynamics, goes beyond the Born-Oppenheimer approximation, where due the small mass of the electron, the electronic system is assumed to relax much faster than the core of the atom. Without this approximation the dynamics of the excited electronic system during the interaction of complex ion target combination with many electrons involved, can be probed. However, as a starting point for developing ab initio approach, light and single charged ions are an ideal tool to face this daunting task. The main goal for the experiments presented in the following chapters was to enable comparison of these computations with experiments for a simpler and straightforward system, in an attempt to expand the obtained knowledge later to more complex ion-solid combinations and different processes, as observed in experiments with highly charged ions.

2. Experimental Methods

This chapter will cover the experimental setup of BeamLine1 (BL1) in the Augustin laboratory at TU Wien [37, 38] and explain how BL1 allows the investigation of both energy and charge transfer of ions transmitted through free-standing 2D materials. A schematic of the beam line can be seen in figure 2.1.

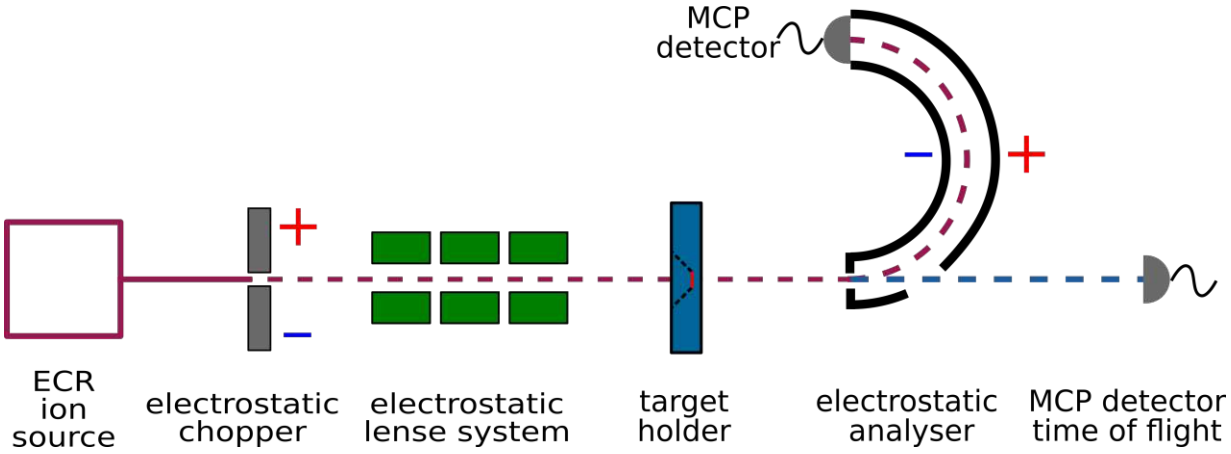

Figure 2.1.: Schematic of BeamLine1 and its key components. At the end two of the beam paths MCP detectors allow to study charged (red) particles using an electrostatic analyser and neutral particles (blue) using a time of flight (TOF) approach, respectively.

The ions for the experiments are produced in an external electron cyclotron resonance ion source and are guided by magnetic fields into BL1. There, the ion beam is first of all chopped by an electrostatic chopper to allow time of flight measurements (TOF) and afterwards the beam is additionally shaped by an electrostatic lens system to guide the ions accurately into the target chamber and onto the sample. After transmission of the sample, the energy of still charged particles is measured in an electrostatic analyser (ESA), whereas for neutral particles a time of flight approach is applied. Multi-channel-plate (MCP) detectors are used for both, neutral and charged particles. A detailed description of the main components follows in the next sections.

2.1. Electron cyclotron resonance ion source "SOPHIE"

In an electron cyclotron resonance (ECR) ion source ions are produced by injecting microwaves into a working gas in an external magnetic field. A schematic can be seen in figure 2.2 If the alternating field of the microwave coincides with the gyration frequency of the electrons in the given external field, their kinetic energy is increased. These hot

electrons then collide with the working gas and create ions by impact ionisation. This processes does not only generate singly ionised atoms, but also higher charge states.

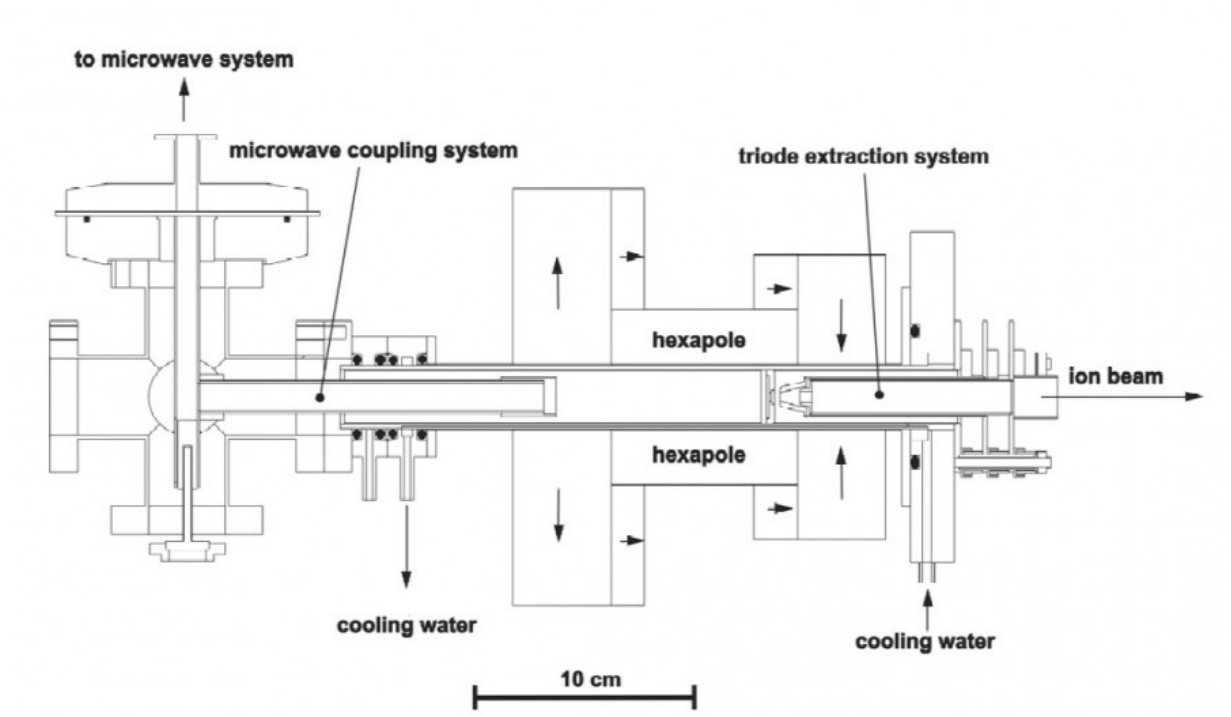

Figure 2.2.: Schematic of an electron cyclotron resonance ion source, displaying the coupling of the microwave source to a chamber filled with a working gas and the extraction system. Image adapted from [39].

The particular ion source used for the experiments described here ("SOPHIE") operates with microwaves in the range of 12.75 GHz to 14.5 GHz and uses a plasma confining field consisting of only permanent magnets [39]. A triode extraction system allows for ion acceleration voltages between 500 V and 5 kV. The extracted ions are then separated according to their mass to charge ratio by a sector magnet, allowing the selection of the desired ion species and charge sates. An additional set of quadrupole magnets can be used to further shape the ion beams, before they are guided into BL1.

Electrostatic lens system

After the ion species of interest hast been selected from the sector magnet, a electrostatic lens system allows to additionally shape and deflect the ion beam. It consists of three sets of lenses, each set itself is composed of two pair of electrodes. One pair for a horizontal and the other for a vertical electric field inside the set.

2.2. Detection of charged particles

As a way to quantitatively investigate the ion-solid interaction, ions of a well defined energy are introduced into the system and by subsequent measurement of the ion's energy after the interaction with the solid, the energy transfer is determined. Here, the energy ions is measured by utilizing the energy dependence of the trajectory of a charged particle in an homogenous transverse electric field in.

Electrostatic analyser

An electrostatic analyser (ESA) is a powerful tool to precisely measure the energy-to-charge ratio of charged particles. In essence, it consists of two cylindrical metal plates, placed concentric with different radii (figure 2.3) with small slits at both ends. By applying different potentials to the plates an electrostatic field is created, forcing charged particles on a circular trajectory that depends on the energy and charge of the particles. If the applied voltage for a given ratio $\frac{E}{q}$ is too low, the particle crashes onto the outer plate, if it is too high it crashes onto the inner plate. Only for a certain voltage U_{pass} the trajectory is on a concentric circle exactly in the middle of the two plates and is not blocked by neither, the entry or exit aperture, allowing the particle to pass the ESA and hit a detector. Thus only a particle with charge q and energy E can pass the ESA and consequently is able to get detected if the relation of:

$$U_{\text{pass}} = g\frac{E}{q} \tag{2.5}$$

is fulfilled, where g is a geometry factor dependent on the curvature of the plates in the ESA. For the "Comstock Electrostatic Energy Analyser, ESA90XB-MAN-0495" used in this experiment $g = 0.43$.

Thus when gradually varying the potential between the plates, an energy distribution of a beam of charged particles can be obtained. In the case that the incoming ions are multiply charged ($q > 1$), the ESA also allows to observe charge changes in addition to the energy measurement. It is important to note, that even if in principle only the ratio $\frac{E}{q}$ of the particles can be measured, the stopping and charge exchange can usually be easily distinguished in the spectra. For this reason an ESA is an ideal tool to characterise a beam of charged particles.

In the experiments here, the applied deflection voltage on both plates with equal magnitude but opposite polarity is slowly ramped up while a MCP detector at the other end of the ESA counts the deflected ions at the corresponding voltage. Another MCP detector at the end of the chamber keeps track of the neutral atoms ($q = 0$) that are not deflected and pass the ESA in a straight line, see figure 2.3. Both MCP detectors are connected to an in-house build counter, converting the analogue current of the detector in particle counts per second.

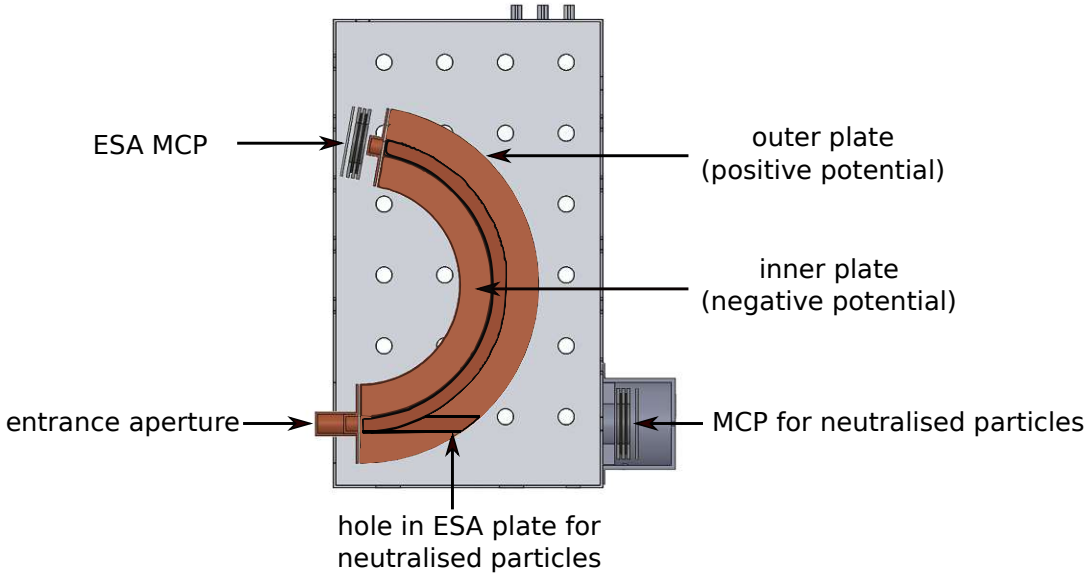

Figure 2.3.: Cross section of the ESA in its shielding box. MCP on top for charged ions that pass the ESA. MCP on the right outside the box for neutral particles.

Both, the deflection plates and the detectors are controlled and read out with a "LabView" program. This software features two parallel readouts, allowing for simultaneous real time comparison of charged and neutralised particles. If desired, the measurement can be repeated several times and by taking an average a more stable result can be achieved. This can be especially useful for low transmission rates, considering that the MCPs are very noise susceptible. Exemplary spectra for 2 keV and 4 keV H^+ ions without transmission of an y sample as measured with the ESA can be seen in figure 2.4.

One important limitation on the energy determination is imposed by the small entrance aperture (and the finite seize of the detectors) of the ESA. While a small opening favours for a more precise measurement of the particles that happen to pass the aperture, as their path is better defined, at the same time, the detectors are only able to detect ions leaving the target in a tiny, solid angle. For that reason, this setup only allows for determination of forward scattered particles. Since particles with a larger scattering angle are usually accompanied by a larger energy loss, compared to ones scattering with a small angle, this setup will underestimate the average transferred energy.

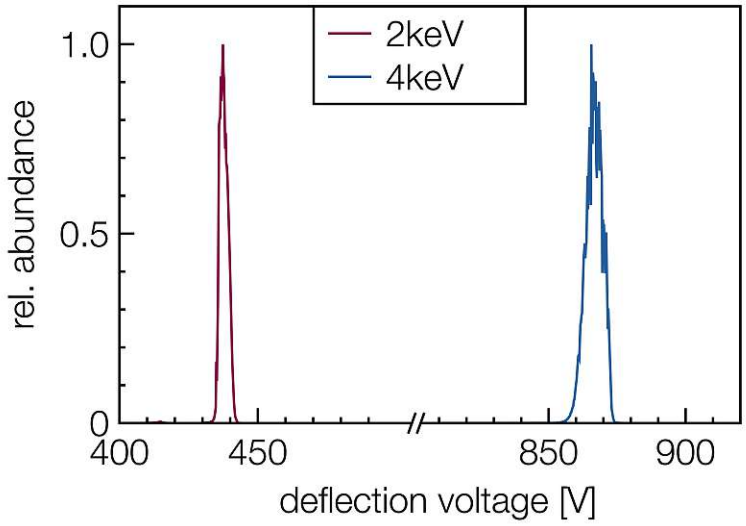

Figure 2.4.: ESA spectra for H^+ ions with different kinetic energies without transmission of any sample. Red: ions with a kinetic energy of 2 keV, blue: ions with a kinetic energy of 4 keV.

Micro-channel-plate

For the experiments described here Micro-channel-plate detectors (MCP) were used. In these kind of detectors, a weak electronic signal produced by an incident particle is greatly magnified by an electric field, acting as an electron multiplier. The electric field accelerates charge carriers produced by the primary particle and these charge carriers produce themself more particles, resulting in an avalanche of electrons, accomplishing an enormous gain. As a MCP detects only secondary electrons, it can be used as a general particle detectors, being even able to detect neutral particles, elusive in other detector types due to the lack of electromagnetic interaction. The combination of high gain, universal particle detection and very similar sensitivities over a large energy range of the incident particles, makes them the perfect choice for experiments investigating the neutralisation of low ion currents.

2.3. Detection of neutralised particles

When an ion interacts with matter, not only energy but also charge can be transferred, possibly neutralising the ion. Due to the lack of an electric charge, the approach described in the previous section to quantify the energy transfer is not applicable to neutral particles, requiring an alternative characterisation method.

Time of flight

In order to determine the energy of neutralised particles a time of flight (TOF) approach is used here. In principle a TOF measurement works as follows: At a start signal, a particle is introduced into the target chamber and once it reaches the end gets detected, a stop signal is produced. The time difference is the TOF of that particle, and for known particle mass and flight length the energy of the particle can be determined:

The kinetic energy of ions in the charge state q_{ion} produced within the ECR source and accelerated by a voltage of U_{source} is given by:

$$E_{kin}^{(0)} = q_{ion}\, U_{source} = \frac{m\, v^2}{2} \tag{2.6}$$

with m and v being the ion's mass and velocity respectively. With a given flight distance d from the target to the detector, the TOF of a particle not interaction with the target thus is:

$$TOF^{(0)} = \frac{d}{v} = d\sqrt{\frac{m}{2\, E_{kin}^{(0)}}} \tag{2.7}$$

If the time of flight is greater than this (i.e. $TOF' > TOF^{(0)}$), the transfer of the kinetic energy from the ion to the sample results in:

$$\Delta E = E_{kin}^{(0)} - \frac{m\, d}{2\, TOF'^2} \tag{2.8}$$

In principle, in this setup it is only possible to measure the $TOF_{chopper\text{-}detector}$, but since the $TOF_{chopper\text{-}target}$ is the same, regardless if the ion interacts with the sample or not, it can be subtracted as an offset, as the interest is in the $TOF_{target\text{-}detector}$.

In this setup, an electrostatic chopper (figure 2.5) supplied by fast electronics is used to produce short ion pulses. Usually the chopper deflects ions, preventing the beam from entering the chamber. But once a start signal is sent, the choppers' deflection voltage is turned off for a few nanoseconds. After passing the chopper, ions interact with the samples in the target holder and lastly, the particles hit a MCP detector at the end of the chamber, producing the stop signal for the TOF measurement. Start and stop signal are the input for a Time-to-Amplitude Converter (TAC). The TAC outputs a voltage linearly proportional to the time difference between start and stop, therefore the TOF. A schematic diagram showing signal progression and all electronic devices can be found in figure 2.6.

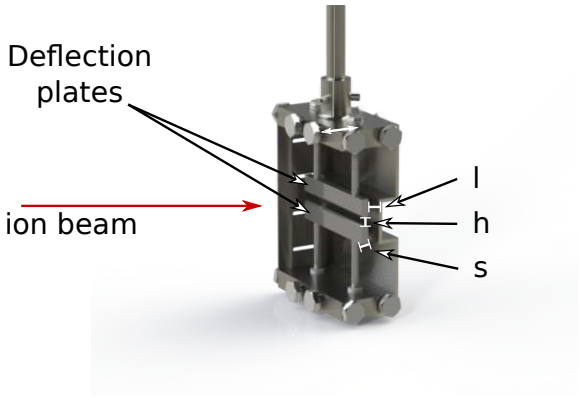

Figure 2.5.: The electrostatic chopper. By applying a voltage on the two deflection plates, ions can be prevented from passing the chopper. The length of the deflection plates in beam direction s, the space in-between h and the distance to the aperture l are denoted.

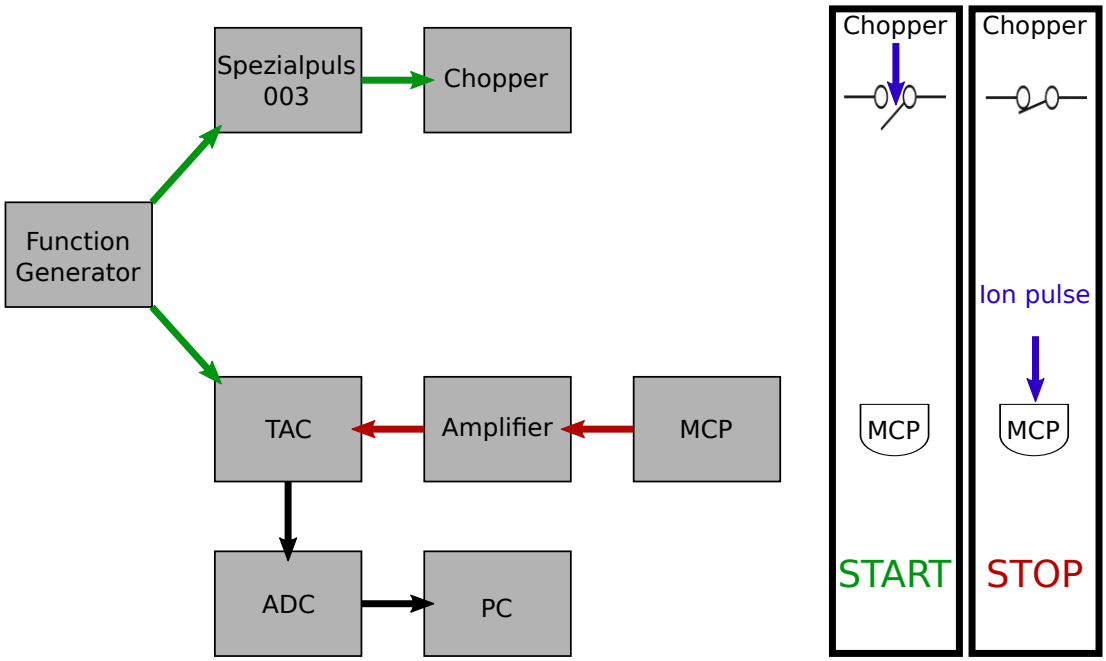

Figure 2.6.: Schematic signal propagation of a TOF measurement. The start signal is generated by a function generator is both, the trigger signal for the "Spezialpuls 003", that causes the chopper to open, and the start signal for the TAC. When an ion pulse is detected on the MCP, the amplified output is the stop signal for the TAC. From the time difference between those two input signals, the TAC outputs a proportional signal, that is converted by an ADC and finally is evaluated by a PC.

Start signal

The TOF measurement starts with an "Exact® model 119 function generator" producing a +10 V square-wave signal. This signal fulfils two purposes: Firstly, it serves as a start signal for the "Ortec® Time-to-Amplitude Converter 566" (TAC). Secondly, it is the trigger signal of the chopper's electronics, the "Spezialpuls 003", prompting the deflection plates to briefly turn off, thereby creating an ion pulse that enters the chamber. It is important to note, that the frequency of this trigger signal has to be smaller than the inverse value of the expected TOF, preventing multiple ion pulses to be in mid-flight in the chamber.

The Spezialpuls' output has to be shaped by four tunable resistors. These are responsible for: the opening pulse width, the delay for the cut-off pulse and to take account of the contact impedance of each deflection plate. The adjustment of these have to be done with great care: Not only are the properties of them dependent of each other, but also even small tuning can lead to huge changes in the chopping process.

While a short opening time is desired for a sharp ion pulse, it is important that it is long enough for ions to pass the deflection plates during that time. Considering the length of the chopper in beam direction $s = 2$ mm (figure 2.5) and the time light ions need to pass it, the opening time has been set to approximately 10 ns (figure 2.7). Additionally

the deflection of the beam Δy must be larger than the next aperture after the chopper in order to fully block incoming ions. The deflection for an ion with charge q, mass m and velocity v is given by [40]:

$$\Delta y = \frac{U_{choppper}\, q\, s}{h\, m\, v^2} \left(\frac{s}{2} + l\right) \tag{2.9}$$

with h being the spacing between the two deflection plates and l being the distance between chopper and aperture. Typical bias voltages are between ±5 V and ±50 V.

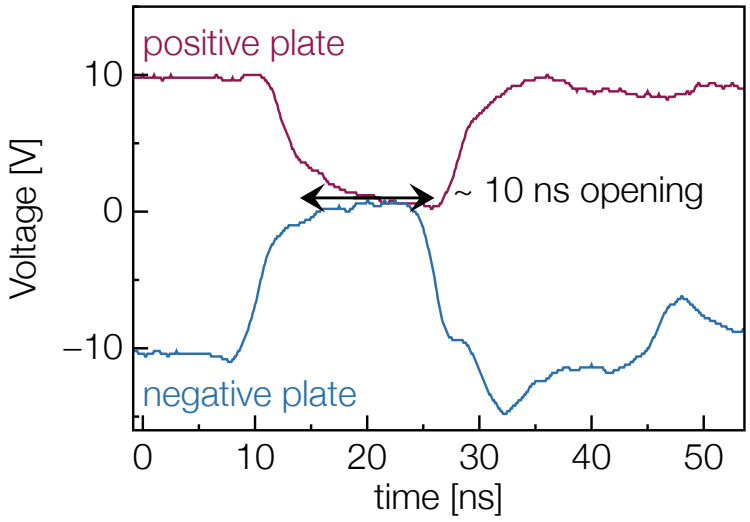

Figure 2.7.: Voltage applied to the two deflection plates over the course of one chopping process.

Stop signal

After the ion interacts with the sample, it hits the MCP at the end of the chamber. The MCP signal gets amplified by a "Winkelkemper engineering® pad 01s preamplifier/discriminator" and provides the stop signal for the TAC. The threshold of this amplifier has to be adjusted to minimize noise while still accepting the signal of incoming ions.

TAC and time of flight

The signal from the function generator and the MCP signals are used as the inputs of the TAC. The TAC then outputs a signal with its amplitude proportional to the time between start and stop signal, thus the TOF. Examples can be seen in figure 2.8. This signal is then ultimately transmitted to the PC via a "CAEN ® N957 8k-Multi-Channel Analyser" analog to digital converter (ADC). Using the CAEN ® software "N957 Tool" the ions' TOF can be acquired while also creating a fast histogram, dividing the signals over "pulse height bins".

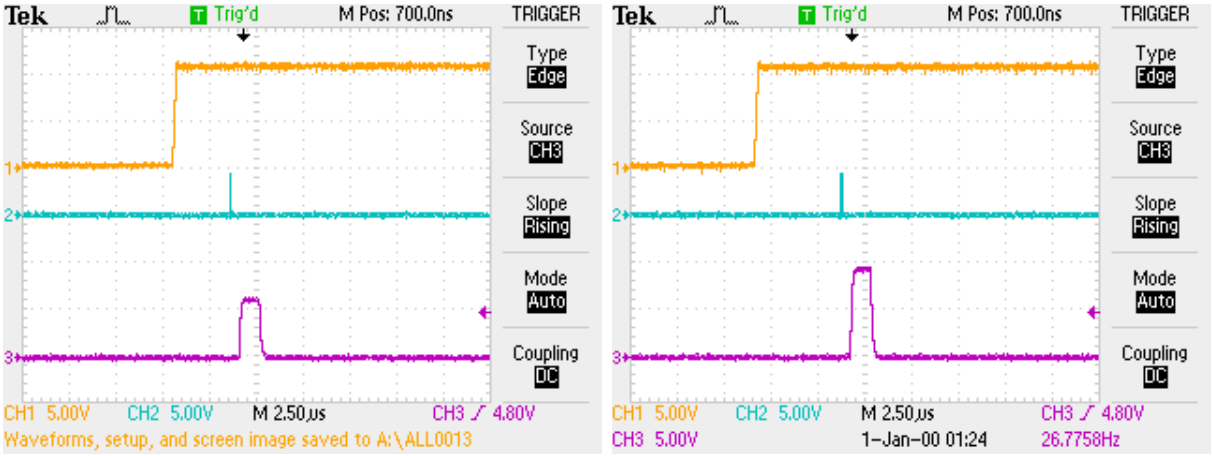

Figure 2.8.: The time difference between the function generator's start signal (yellow) and the MCP's stop signal (blue) determines the TAC's output height (purple). Voltages have different offset for better visual clarity. Example signals are given for (a) short TOF and (b) long TOF.

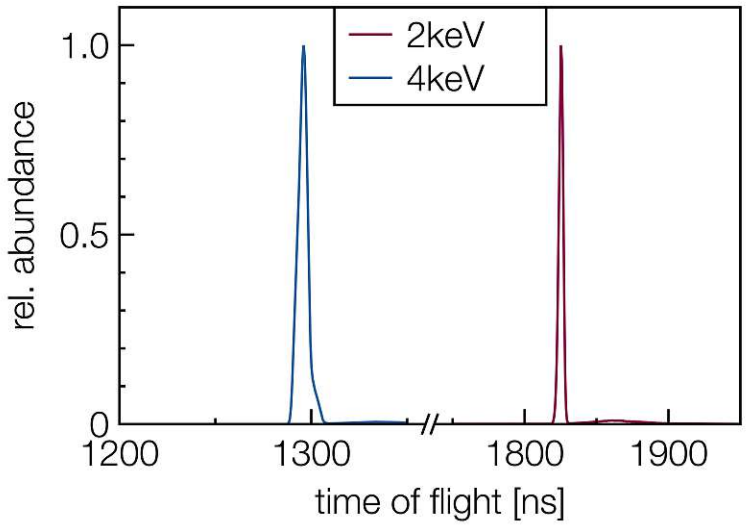

Figure 2.9.: TOF spectra for H^+ ions with different acceleration voltages. Red: ions with a kinetic energy of 2 keV, blue: ions with a kinetic energy of 4 keV.

The most challenging part of this setup is to proper calibrate all the electronics to work for different ion energies and with a new aligned beam exiting the source. Starting with the frequency of the function generator, to tuning the four resistors and picking a fitting deflection voltage, there are many parameters that are not independent of each other. Unexpectedly the chopper frequency also had an effect on the efficiency the chopping process. Even more surprising is, the sharpest TOF spectra were achieved at relatively high frequencies, close to the fundamental limit of $f_{generator} < \frac{1}{TOF}$ (to guarantee that at any time, only one ion pules is present in the chamber).

2.4. Target holder and transfer chamber

For the experiments discussed here a suitable target holder was designed using the CAD software "Solid Works" and manufactured by the workshop at TU Wien. The individual pieces and their names used within for this chapter can be found in figure 2.10. It features holes for four samples to be mounted onto, allowing ion transmission through free-standing 2D samples. To make fast sample changes possible without breaking the vacuum in the main chamber, the target holder was designed to get picked up by a transfer rod and moved into a transfer chamber behind a UHV gate valve. The transfer chamber is equipped with its own pump. Furthermore the target holder needs to allow for heating of the target plate in order to clean the samples properly, while also measuring its temperature. This is achieved by using a heating wire and a platinum resistance thermometer (PT100), respectively. Additionally the target plate is grounded, preventing it from becoming electrostatically charged when exposed to an ion beam while at the same time estimating the beam current. In order for these functions to be used while also allowing the target holder to be transferred out of the vacuum chamber, a SUB-D 9-Way UHV ceramic socket was used to connect the mobile head piece with the fixed manipulator piece. The pins where crimped according to figure 2.11.

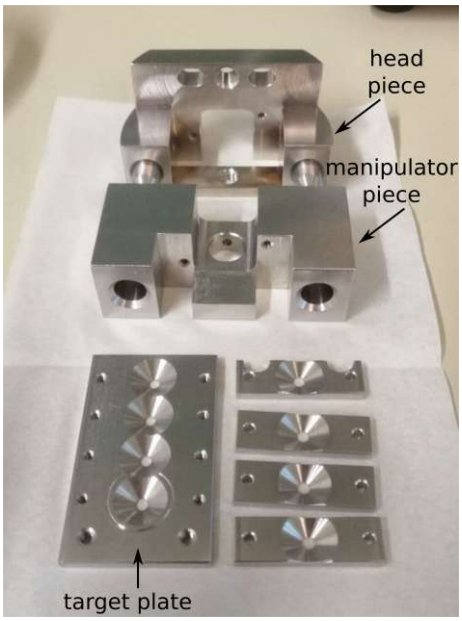

Figure 2.10.: Individual parts of the target holder. Top: Head piece with bolts to be inserted into the manipulator piece and with a screw hole to connect it to a transfer rod. Middle: Manipulator piece which is permanently mounted on the manipulator inside the main chamber. Bottom: Target plate with space for four samples to be clamped onto using the smaller plates.

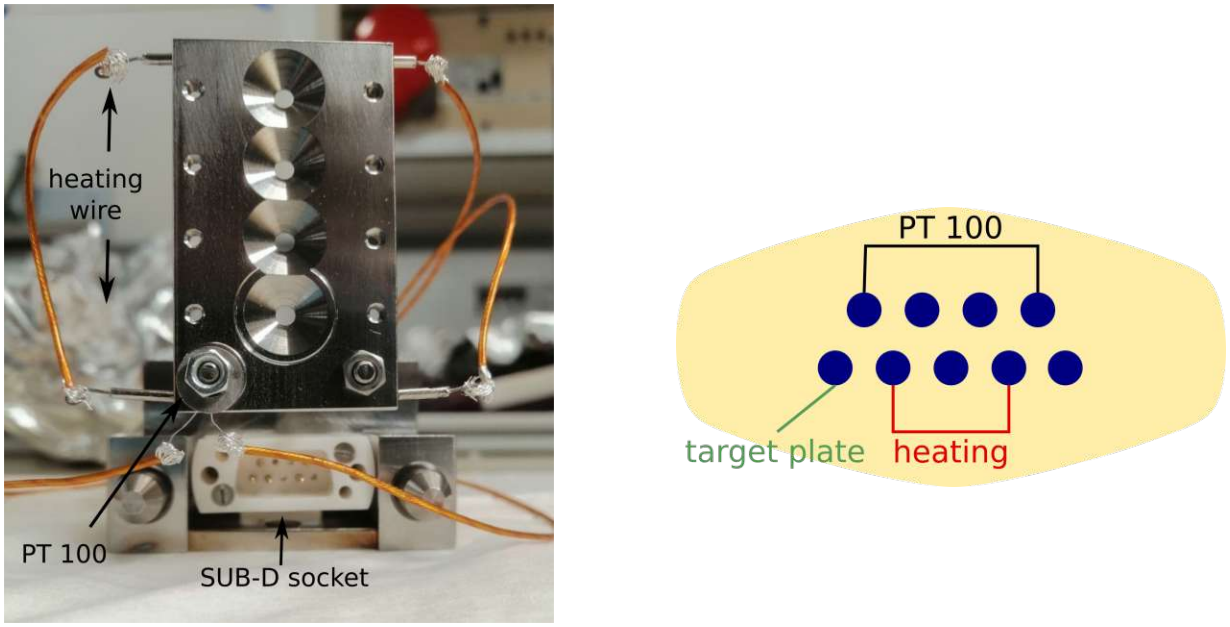

(a) (b)

Figure 2.11.: (a) Target holder fully assembled. (b) SUB-D (female) pin assignment.

2.5. Samples

To prepare free-standing 2D materials suitable for experiments, the material of interest is deposited on a substrate for support. This prevents the otherwise fragile 2D material from tearing, bending or sticking to itself. The samples used here are placed on Quantifoil, an approximately 10 nm thick carbon mesh with holes of a diameter of about 2 µm (figure2.12). The Quantifoil itself is mounted on transmission electron microscopy (TEM) grids, a much coarser, around 95 µm wide mesh made of gold. Where both those holes overlap it is possible to investigate exclusively free-standing 2D materials. However, in the experiments described here the ion beam diameter is much wider than the 2 µm wide opening of the Quantifoil, leading to unavoidable interaction of ions with the substrate. While this effect can be observed, the contribution to the measurement when regarding the ion energy loss is small and can be distinguished from interaction with the free-standing 2D sample.

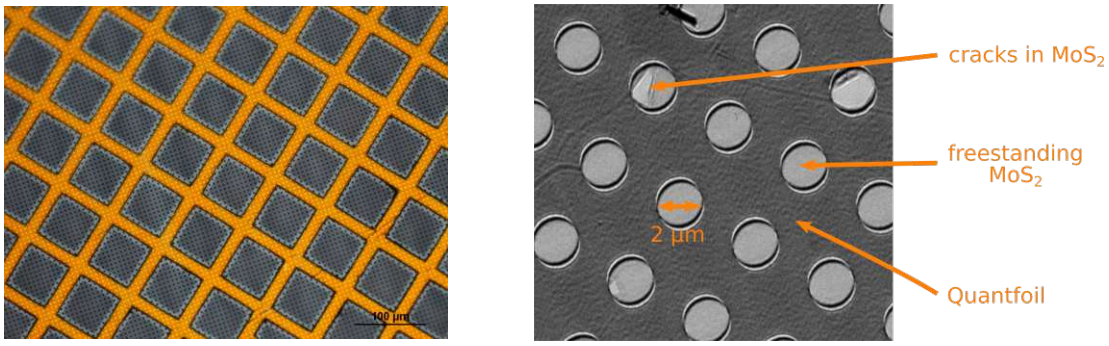

Figure 2.12.: Left: Image of SLG on golden TEM grids and Quantifoil [41]. Right: Scanning transmission electron microscopy image of MoS_2 supported on Quantifoil.

To estimate the energy loss of ions passing through the Quantifoil, TRIM simulations of ions transmitting a thin layer of carbon, exemplary for the Quantifoil support, were made. The resulting energy loss of transmitted ions with a deflection angle small enough to get detected in the experiment was then compared to the TOF measurements. Good agreement was found with the experiment for a simulated 8.5 nm thick carbon layer. As can be seen in figure 2.13 the energy loss of the support separates well from the free-standing 2D sample, what allows to analyse the energy loss of the 2D sample without distribution from the support. On the other hand, the effect of the TEM gird on the ion beam is not visible in the experiment. Most ions simply pass without any interaction at all due to the coarseness of the grid and the few ions that indeed hit the grid transfer to much energy and get deflected at a too large angle to interfere with the measurement.

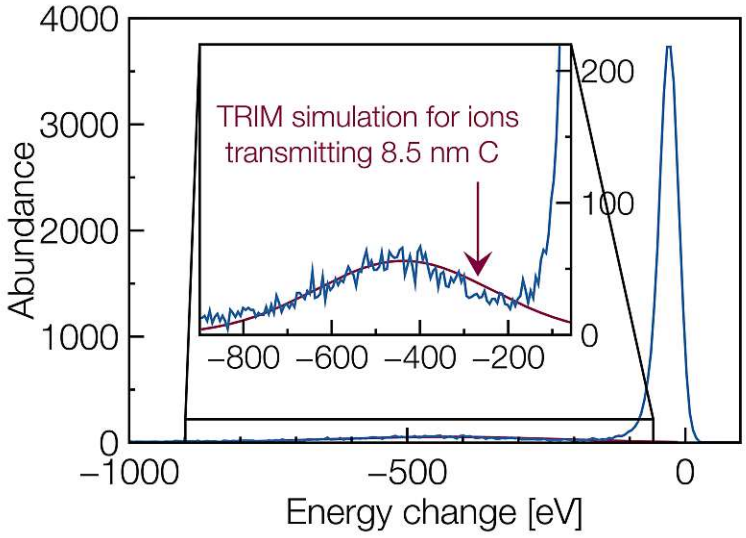

Figure 2.13.: Energy transfer of H^+ accelerated by 3 kV transmitted through a SLG sample compared with angle-filtered TRIM simulations for 3keV H^+ transmitted through 8.5 nm thick carbon, exemplary for the Quantifoil support. The Quantifoil support is apparent in our measurements.

Another challenge that arises when investigating free-standing 2D materials is that, due

to their atomically thin nature, they are especially susceptible to surface contaminations, as even a small amount of foreign material can dominate the here investigated properties the sample. These contamination cannot only originate from exposure to air or rest gas in vacuum chambers but can also be ascribed to residuals of polymers used in the manufacturing process [42]. By heating the samples to 350°C a noticeable change in the time of flight spectrum of ions traversing the 2D material can be observed (figure 2.14). Not only is the amount of detected ions transmission through the sample greatly increased, the spectrum is also narrower and shifted towards shorter times of flight, indicating less unwanted scattering events and energy transfer processes with contaminations. This agrees well with the cleaning mechanism of 2D materials described in [43]. The effect of surface contamination on transmitted ions is roughly comparable to a 1nm thin layer of carbon as estimated using TRIM.

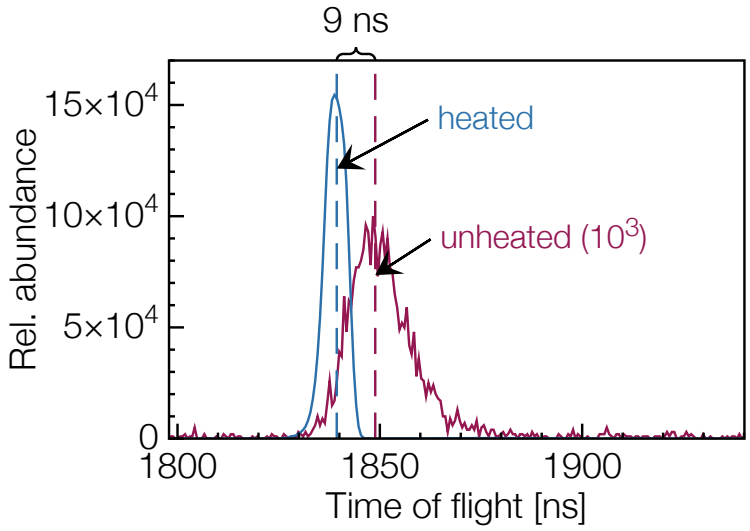

Figure 2.14.: Time of flight of H^+ accelerated by 2 kV transmitted through SLG. Red: unheated sample, magnified by 10^3. Blue: sample after heating to 350°C. The time of flight difference is 9 ns, which corresponds to an energy transfer of 47 eV. The effect of the contaminations on the transmitted ions is equivalent to 1 nm of carbon.

The SLG samples were commercially acquired from "Graphenea", whereas the MoS_2 samples were prepared at Jena University (group of A. Turchanin) and transferred on the TEM grids at the University of Vienna (group of J. Kotakoski).

3. Results and Discussion

This chapter summarises the execution and results of the experiments conducted during this work.

In the beginning, the method of measurement is addressed in detail, with a focus on how samples and ion beam were characterised at the beginning of each experiment.

Later, the results of measurements on SLG and MoS_2 with different ion species and varying initial kinetic energies are brought together and discussed.

In the end of this chapter, comparisons to time depended density functional theory (TDDFT) calculations by collaborators at the Institute of Ion Beam Physics and Materials Research, Helmholtz-Zentrum Dresden-Rossendorf (HZDR) are made. These Ehrenfest dynamics simulations are done using the GPAW package.

3.1. Measurement procedure and sample characterisation

Once the ion source was tuned to produce a sufficient ion current and the chopped ion beam was properly aligned in BeamLine1, a first energy profile of the ion beam with retracted target holder was measured in both, the ESA and TOF. This confirms that the mean ion energy is in agreement with the source settings and with each other, while additionally verifying that the energy width is as small as possible by fine-tuning the magnetic and electric fields shaping the ion beam before the chopper. The results were later used as a point of reference for the transmission experiments. This calibration was redone every time the control parameters of either the ion source or the beam optics were readjusted, to ensure that the effect of different beam geometries will not influence the measurement.

With this well-defined ion beam, the heated target holder was moved down in the chamber with the one sample to be measured at the approximate centre of the beam. Then the transmitted ion energy profile was measured anew and compared to the previous defined references. The results were again fitted with a Gaussian distribution to determine the mean energies, the difference to the reference measurement being energy transferred from the ion to the sample. Even if the transmitted ion energy distribution was expected to be described my a Moyal function, there was a better agreement for a Gaussian fit. The simultaneous measurements in the ESA and TOF (i.e. charged and neutral particles respectively) for identical beam parameters yield a charge exchange dependent measurement of the transferred energy of ions transmitting the 2D sample.

Additionally, the resulting spectra also give a first characterisation of the 2D samples, as the sample coverage can be estimated by comparing the abundance of transmitted ions with and without energy loss. In the case of a sample with some holes or cracks within the 2D material, the spectra of transmitted ions are separable (i.e. two distinct Gaussian distributions are identifiable), with of one distribution showing no energy change, resembling the ion beam measured without a target, and the second distribution displaying an

finite energy loss. These different contributions can be ascribed to ions passing the sample through defects (holes and tears) and ions transmitted through the intact 2D material respectively. Comparing the area under the Gaussian bell of those different distributions over the same time period leads to an approximate coverage of the 2D sample.

For most Graphene samples the coverage was close to 100%, displaying a single Gaussian distribution in transmission (figure 3.1), whereas for MoS_2 the coverage was varying and considerably lower. An exemplary ESA spectrum of MoS_2 with noticeable gaps in the sample can be seen in figure 3.2. Those results can be qualitatively compared with the STEM data, where cracks in layers were visible in the case of MoS_2 as discussed in section 2.5.

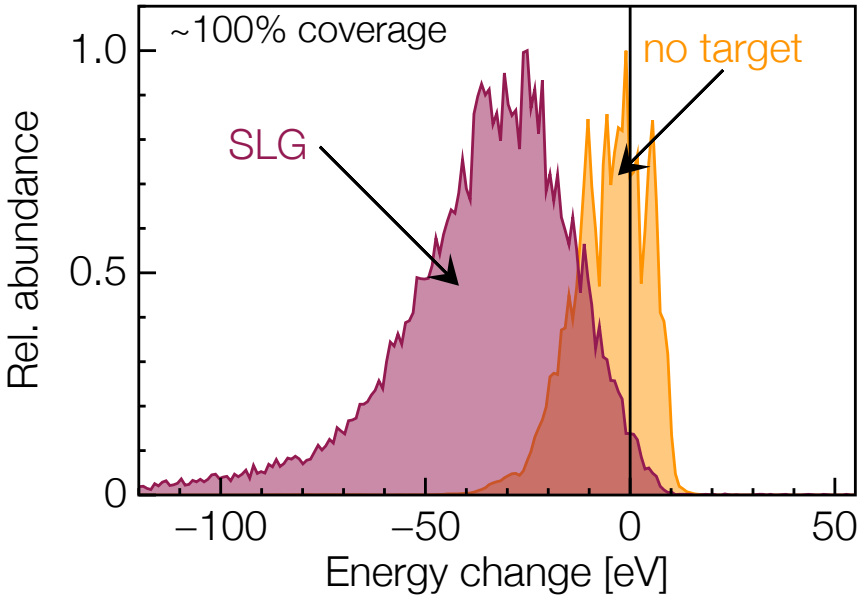

Figure 3.1.: ESA spectrum for 3keV H^+ transmitted through SLG (red) and compared to the ion beam without target (orange). The dashed vertical line is the energy change simulated with TD-DFT calculations. For ions transmitted through SLG only one distribution is visible, indicating high sample coverage.

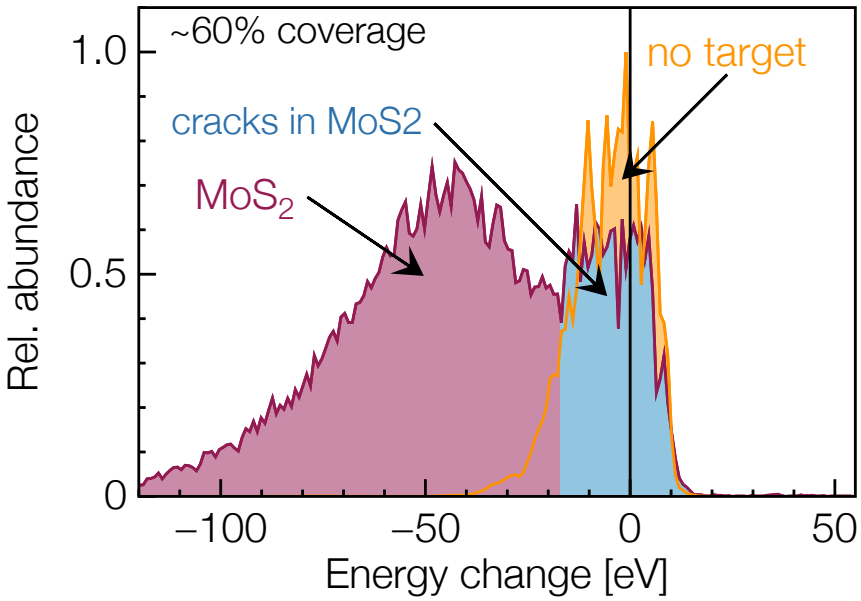

Figure 3.2.: ESA spectrum for 3keV H^+ transmitted through MoS_2 (red) and compared to the ion beam without target (orange). Parts of the energy distribution of the ions transmitted through MoS_2 resembles the distribution without sample and are ascribed to ions passing holes in the MoS_2 (blue), indicating imperfect sample coverage.

Furthermore, since the TOF MCP is placed behind a small hole in the backplate of the ESA casing, the TOF measurements can be conducted in two modes of operation. If a voltage is applied on the ESA deflection plates, the TOF spectrum only contains neutral particles (normal mode). But if the deflection plates were grounded, the TOF contains both, neutrals and still charged particles instead (mixed mode).

Comparing the particle flux of those two modes of operation, allows to draw conclusions about the neutralisation probabilities and charge dependent energy loss (figure 3.3). Here can already be seen, that the neutralised particles have a higher tendency to transfer more energy then the their still charged counterpart. However it is important to note, that even if the spacial orientation and the energy profile of the ion beam is usually constant over multiple days and thereby longer than a typical measurement of several hours, the ion current could change by a sizeable amount, most likely due to fluctuations in the pressure of the working gas, leading to imprecise results for the neutralisation probabilities.

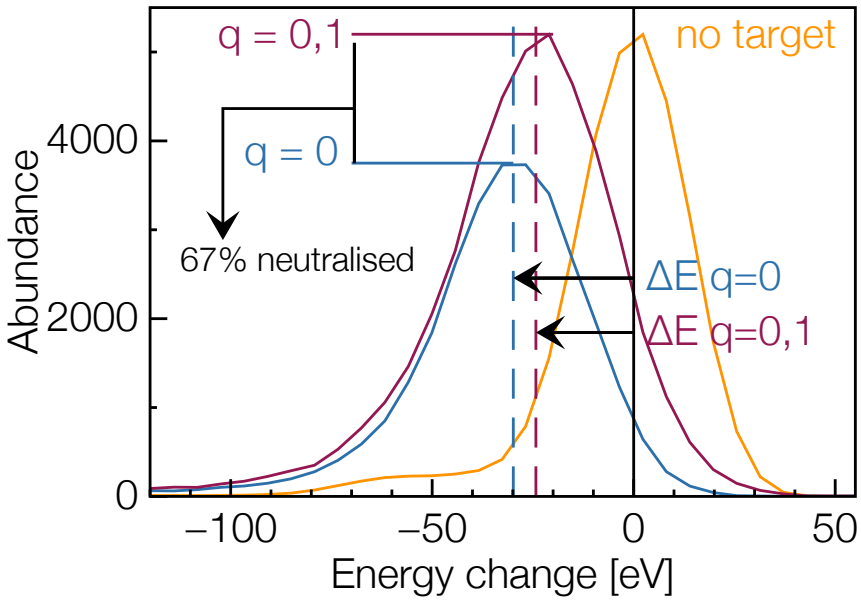

Figure 3.3.: TOF spectrum for 3keV H^+ transmitted through SLG compared to the ion beam without the target (yellow). TOF measurement were done in different modes of operation: Filtering for only neutralised particles (blue) and a mixture of neutralised and charged particles (red). The comparison yields an estimation of the neutralisation probability of ions transmitted through the SLG.

3.2. Error analysis

The ion current and thus detected counts were in the range of 10 000 cps, resulting in good statistics. The standard error for both measurements were < 1 eV.

To get an estimation of the precession and time stability of the measurements, control measurements were done and repeated ten times over multiple days - a timespan much longer than a typical measurement that only takes hours. This leads to an additional error of $\sim$1 eV in the ESA and 1-5 eV, depending on ion velocity, in the TOF measured energy transfer.

In the ESA a possible contribution to the error is rooting from the incident angle of the ion beam. This has been estimated by small variations of the deflection voltages, resulting in an error of 6eV

For the TOF measurements, an additional source of uncertainty was given by the chopping electronics, though it is still unclear if it roots in the function generator or the "Spezialpuls 003". Certain is, that an issue manifested itself in the form of an absolute timeshift in the chopping of the beam. The chopping timing could vary on a scale of a few ns which leasd to an error that was highest for the fastest ions (i.e. hydrogen at 5 keV) resulting in a maximal error of $\sim$20 eV.

3.3. Energy transfer

The measurements described in section 3.1 were repeated for various ion species and for up to five different initial kinetic energies, ranging from 1 keV to 5 keV. The results are summarised in figure 3.4 and 3.5 for SLG and MoS_2 respectively. In both figures the transferred energy for hydrogen ions is left and for helium ions right. The results are separated by charge state and thus analysation technique. Blue points being neutralised particles, with data acquired using the TOF and orange points are still charged ions studied with the ESA.

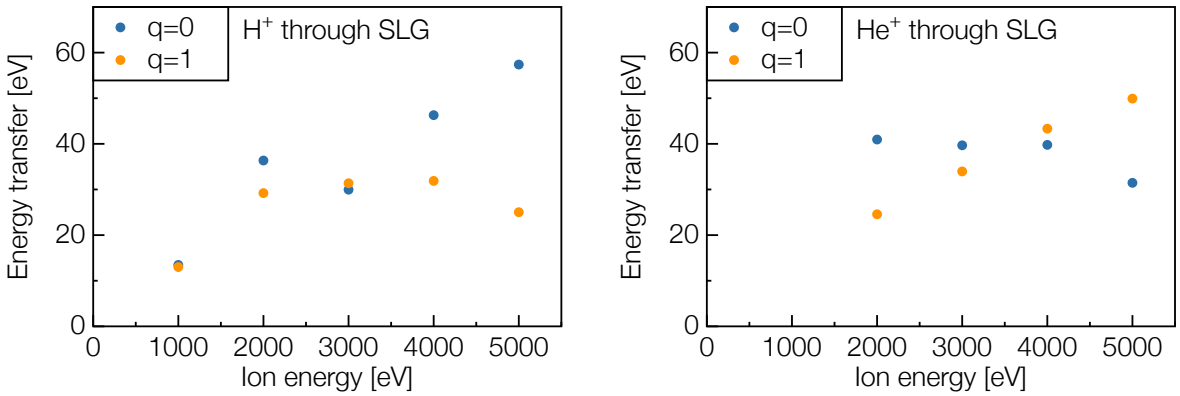

Figure 3.4.: SLG target: Transferred energy of neutralised (blue) and still charged (orange) H^+ (left) and He^+ (right) ions transmitted through SLG.

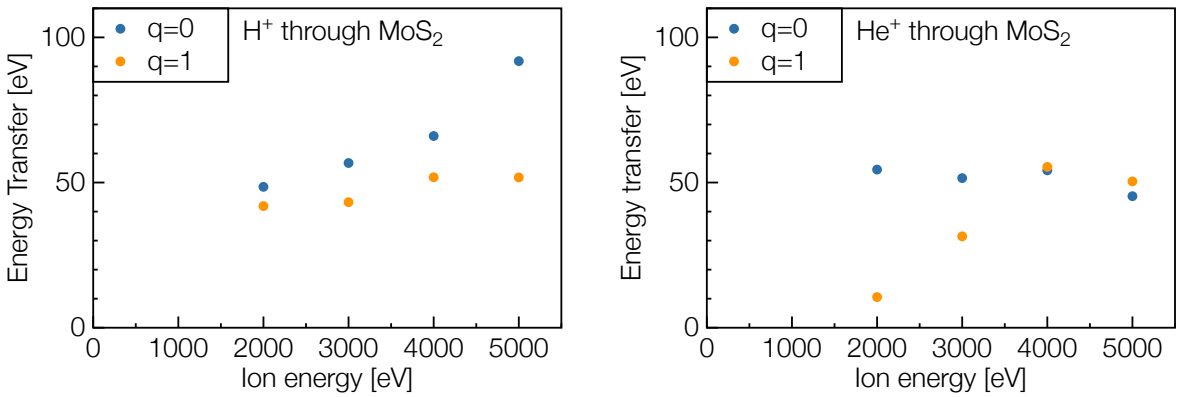

Figure 3.5.: MoS_2 target: Transferred energy of neutralised (blue) and still charged (orange) H^+ (left) and He^+ (right) ions transmitted through MoS_2.

A general trend of higher transferred energies with increased initial ion energy can be observed, although especially ions neutralised in MoS_2 deviate from this behaviour. The relative energy transfer however, tends to be maximal for the lowest energies. Notably the energy transfer of fully neutralised particles appears to exceed their still ionised counterparts.

3.4. Discussion and comparison with TD-DFT simulations

If the transferred energy is considered as a function of ion velocity instead of kinetic energy (as was presented in section 3.3), a linear dependence can be recognized, as can be seen by the circles in figures 3.6 and 3.7, where filled and empty circles are the measured values of the charged and neutralised particles respectively. A linear behaviour in dependence of velocity and atomic number is expected by Lindhard-Scharff theory for ion stopping by interaction with an electronic gas described in equation 1.4 [7, 9], and a higher relative energy transfer for slower ions indicate that the interaction time is the crucial quantity for the processes of the interaction in which the energy transfer occurs. A more generalised behaviour between different ion species can be observed, if the transferred energy is normed by $1/Z$, as a screening factor in the limit of slow ions.

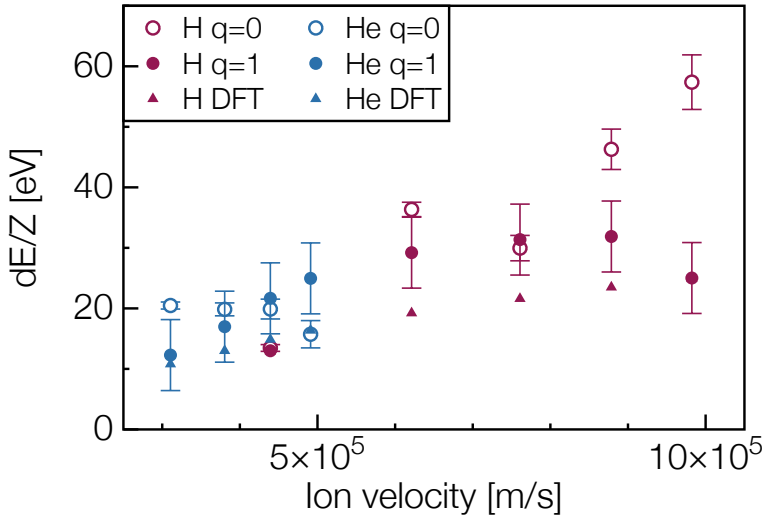

Figure 3.6.: Transferred energy of H^+ and He^+ ions transmitted through SLG divided by Z.

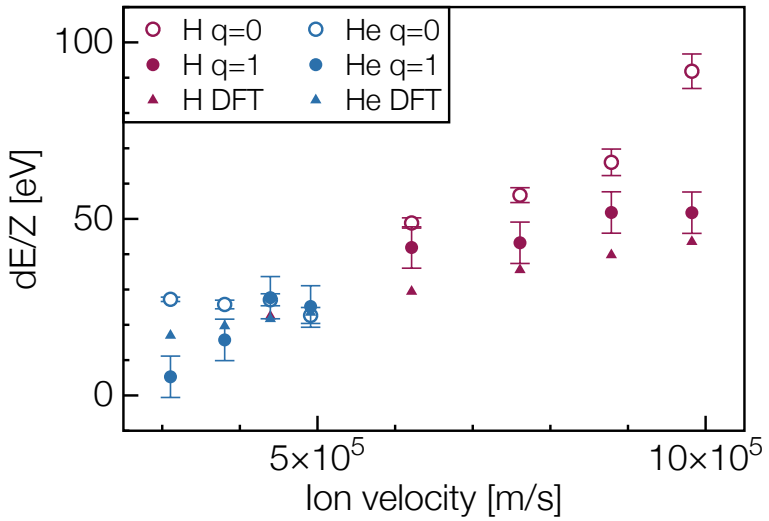

Figure 3.7.: Transferred energy of H^+ and He^+ ions transmitted through MoS_2 divided by Z.

Comparing the above discussed findings with TD-DFT simulations yields similar conclusions, albeit the simulations underestimate the experimental measured energy transfer, indicated by the triangles in figures 3.6 and 3.7. Since the charge state in TD-DFT is not strictly binary, the experimental data for different charge states was combined according to the neutralisation probabilities, depicted in figure 3.8 and 3.9, where a discrepancy of around 50% is can be seen.

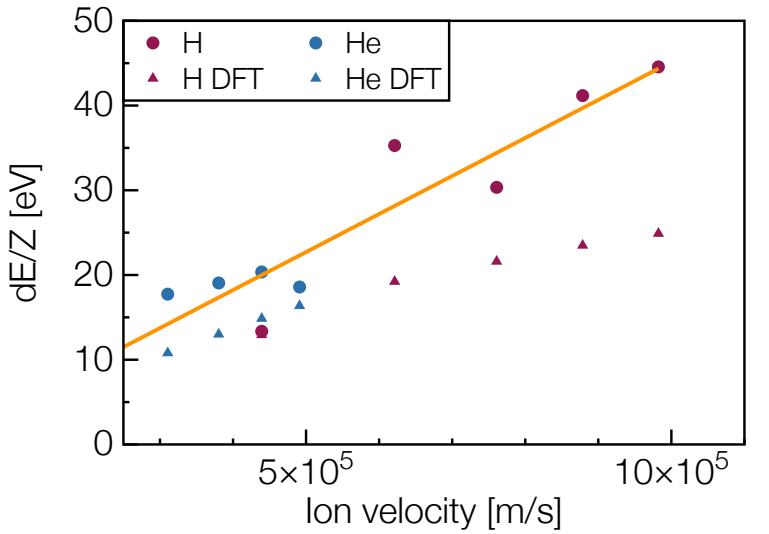

Figure 3.8.: Transferred energy of H^+ and He^+ ions transmitted through SLG. Charge states weighted with neutralisation probability form TD-DFT calculations.

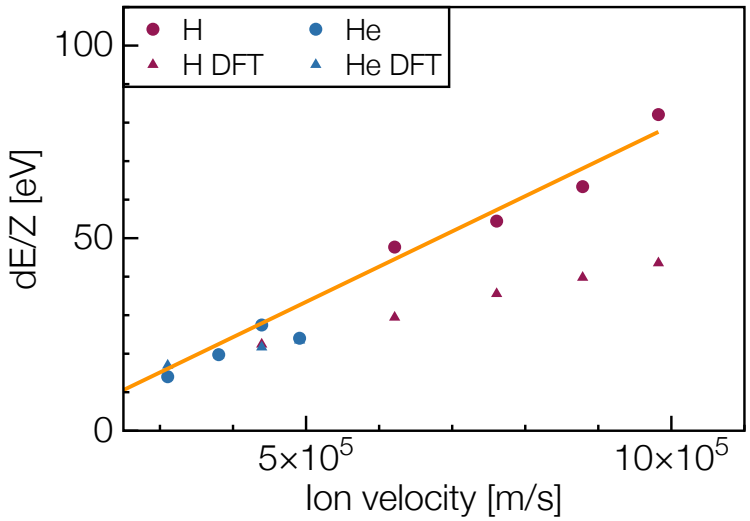

Figure 3.9.: Transferred energy of H^+ and He^+ ions transmitted through MoS_2 . Charge states weighted with neutralisation probability form TD-DFT calculations.

An important experimental limitation that has to be taken into account for any setup realisation is the limited detection angle, enforced by different kind of geometric constraint. For the design in this work in particular, the trade-off between a wide detection angle, and good energy resolution of the ESA has been made in large favour of the energy resolution. The fine aperture in the entrance of the ESA directly lead to a corresponding small acceptance angle of $< 2°$. Thus all data discussed here are only gives information about strict forward scattering. Similar limitations for different reasons are given in simulations, where a larger impact parameter (thus usually smaller scatter angle), is favourable for computational reason, however the bottleneck for comparing both approaches was the experimental acceptance angle. If the results of theory are filtered to the same angle of acceptance angles, as done here, the results become comparable.

4. Summary and Outlook

Goal of this thesis was to finish and optimise the setup at BeamLine1 in the Augustin laboratory, and quantify the energy and charge transfer of light ions transmitting 2D materials, using different techniques for particles that still remain charged and get neutralised during transmission. The experiments were carried out to deepen the understanding of the fundamentals behind ion-solid interaction, with light ions as a simple system that allows comparison to invested state-of-the-art Ehrenfest simulations, with a goal to draw conclusions to more complicated systems such as highly charged ions.

Careful adjustment of all system parameters, especially the tuneable resistors in the "Spezialpuls 003" and frequencies of the function generator for the chopper electronics was required to get precise measurement results. Another important challenge to overcome was discovering a reliable way to guide different ion beams on a well defined geometric path into the experiment using both electrostatic lenses and magnetic fields, thus enabling both stability and reproducibility of the measurements.

The experiments cover hydrogen and helium ions with initial kinetic energies ranging from 1 keV up to 5 keV. The materials of choice were the 2D materials Graphene and MoS_2, exemplary for semimetals and semiconductors.

The different approaches to investigate neutral and still charged particles after transmission, allowed to quantify both, the neutralisation probabilities and the charge dependent energy transfer. Furthermore, this setup can be used as a tool to test the intactness and cleanliness of the 2D samples. It was shown, that the transferred energy has a linear relationship with ion velocity, which is in good agreement with both, Lindhard-Scharff theory of ion stopping as well as more recent TD-DFT simulation using the GPAW code. However in the experiment the absolute energy loss of ions is about 50% higher than in simulations of the before mentioned ion and sample combination. Furthermore the energy transfer of ions which neutralise during transmission is increased when compared to still charged particles. The biggest limitation of the experimental layout is, that only particles in a small angle in forward direction can be detected, thus limiting the conclusions drawn here to only forward scattering.

Future plans for experiments to better understanding of ion-solid interaction using this setup involve using more ion species. The ECR ion source "SOPHIE" is not only able to produce heavier ions but additionally allows to investigate the behaviour of multiple charged ions, as the ESA can distinguish between different charge states, single and multiple electron capture can be analysed. Additionally since the target holder is designed to hold multiple samples and an installed transfer chamber enables quick sample exchange, the study of a variety materials can readily be done, starting from similar systems of multiple stacked layers of graphene up to novel matter of the still growing family of 2D materials.

Danksagung

Zum Schluss möchte ich all jenen danken, die es mir ermöglicht haben, mich diesem Labor einer spannenden Diplomarbeit zu widmen.

Großen Dank an dich, Herbert, dass du stets mit Interesse und Kompetenz die verschiedensten Problemstellungen unterstützend mit mir angegangen bist und wir zusammen mit Paul die bizarrsten Probleme an unserer Quelle und Beamline haben lösen können.

Danke Waldemar, als vorgehender Diplomand warst du der Wegbereiter an Beamline1 und auch wenn unsere gemeinsame Zeit nur kurz war, erinnere ich mich herzlich an die nahe Zusammenarbeit.

Danke Matthias, dass du bodenständigen Rat für mich hattest, sowohl im Labor als auch außerhalb.

Vielen Dank Richard, für deine Inspiration, Geduld und deine Unterstützung, ich bin sehr dankbar, dass ich die Möglichkeit hatte, mich in deiner Arbeitsgruppe zu beteiligen. In meiner Zeit hier habe ich meine Leidenschaft für die Experimentalphysik entdeckt und ausleben können, was den Wunsch auch zukünftig in der Wissenschaft zu arbeiten, nur wachsen hat lassen.

Und natürlich großen Dank an dich Anna, nur durch großes Glück findet man eine Betreuerin, die nicht nur eine so herausragende Physikerin ist, die immer mit kreativen Lösungsansätzen zu helfen weiß, sondern auch eine verlässliche Begleiterin, die mich stets das Beste aus mir herauszuholen schaffte.

Zuletzt ein riesiges Danke an meine Familie, da ihr mir immer ein festes Fundament gibt und mir das Studium erst ermöglicht habt.

Bibliography

[1] E. Rutherford, "Lxxix. the scattering of α and β particles by matter and the structure of the atom," *The London, Edinburgh, and Dublin Philosophical Magazine and Journal of Science*, vol. 21, no. 125, pp. 669–688, 1911.

[2] J. Perrière, "Rutherford backscattering spectrometry," *Vacuum*, vol. 37, pp. 429–432, 1987.

[3] M. Nastasi, J. W. Mayer, and Y. Wang, *Ion beam analysis: fundamentals and applications*. CRC Press, 2014.

[4] J. Melngailis, "Focused ion beam technology and applications," *Journal of Vacuum Science & Technology B: Microelectronics Processing and Phenomena*, vol. 5, no. 2, pp. 469–495, 1987.

[5] J. W. Mayer, "Ion implantation in semiconductors," pp. 3–5, 1973.

[6] K. Kagawa, M. Murakami, Y. Hishikawa, M. Abe, T. Akagi, T. Yanou, G. Kagiya, Y. Furusawa, K. Ando, K. Nojima, M. Aoki, and T. Kanai, "Preclinical biological assessment of proton and carbon ion beams at hyogo ion beam medical center," *International Journal of Radiation Oncology*Biology*Physics*, vol. 54, no. 3, pp. 928–938, 2002.

[7] J. Lindhard and M. Scharff, "Energy dissipation by ions in the kev region," *Physical Review*, vol. 124, no. 1, p. 128, 1961.

[8] S. Creutzburg, A. Niggas, D. Weichselbaum, P. L. Grande, F. Aumayr, and R. A. Wilhelm, "Angle-dependent charge exchange and energy loss of slow highly charged ions in freestanding graphene," *Phys. Rev. A*, vol. 104, p. 042806, Oct 2021.

[9] K. Lindhard and A. Winther, "Stopping power of electron gas and equipartition rule," *Mat. Fys. Medd. Dan. Vid. Selsk.*, vol. 34, 1964.

[10] A. Ojanperä, A. V. Krasheninnikov, and M. Puska, "Electronic stopping power from first-principles calculations with account for core electron excitations and projectile ionization," *Phys. Rev. B*, vol. 89, p. 035120, Jan 2014.

[11] J. F. Ziegler, M. D. Ziegler, and J. P. Biersack, "Srim–the stopping and range of ions in matter (2010)," *Nuclear Instruments and Methods in Physics Research Section B: Beam Interactions with Materials and Atoms*, vol. 268, no. 11-12, pp. 1818–1823, 2010.

[12] J. Enkovaara, C. Rostgaard, J. J. Mortensen, J. Chen, M. Dułak, L. Ferrighi, J. Gavnholt, C. Glinsvad, V. Haikola, H. Hansen, *et al.*, "Electronic structure calculations

with gpaw: a real-space implementation of the projector augmented-wave method," *Journal of physics: Condensed matter*, vol. 22, no. 25, p. 253202, 2010.

[13] K. S. Novoselov, A. K. Geim, S. V. Morozov, D. Jiang, Y. Zhang, S. V. Dubonos, I. V. Grigorieva, and A. A. Firsov, "Electric field effect in atomically thin carbon films," *Science*, vol. 306, no. 5696, pp. 666–669, 2004.

[14] A. K. Geim and K. Novoselov, "The rise of graphene," *Nature Materials*, vol. 6, pp. 183–191, 2007.

[15] A. S. Mayorov, R. V. Gorbachev, S. V. Morozov, L. Britnell, R. Jalil, L. A. Ponomarenko, P. Blake, K. S. Novoselov, K. Watanabe, T. Taniguchi, *et al.*, "Micrometer-scale ballistic transport in encapsulated graphene at room temperature," *Nano letters*, vol. 11, no. 6, pp. 2396–2399, 2011.

[16] A. Akturk and N. Goldsman, "Electron transport and full-band electron-phonon interactions in graphene," *Journal of Applied Physics*, vol. 103, p. 053702, 03 2008.

[17] K. S. Novoselov, D. Jiang, F. Schedin, T. Booth, V. Khotkevich, S. Morozov, and A. K. Geim, "Two-dimensional atomic crystals," *Proceedings of the National Academy of Sciences*, vol. 102, no. 30, pp. 10451–10453, 2005.

[18] K. S. Novoselov, A. K. Geim, S. V. Morozov, D. Jiang, M. I. Katsnelson, I. V. Grigorieva, S. Dubonos, Firsov, and AA, "Two-dimensional gas of massless dirac fermions in graphene," *nature*, vol. 438, no. 7065, pp. 197–200, 2005.

[19] Z. Li, E. A. Henriksen, Z. Jiang, Z. Hao, M. C. Martin, P. Kim, H. L. Stormer, and D. N. Basov, "Dirac charge dynamics in graphene by infrared spectroscopy," *Nature physics*, vol. 4, no. 7, pp. 532–535, 2008.

[20] M. Orlita and M. Potemski, "Dirac electronic states in graphene systems: optical spectroscopy studies," *Semiconductor Science and Technology*, vol. 25, no. 6, p. 063001, 2010.

[21] R. Bistritzer and A. H. MacDonald, "Moiré bands in twisted double-layer graphene," *Proceedings of the National Academy of Sciences*, vol. 108, no. 30, pp. 12233–12237, 2011.

[22] C. Lee, X. Wei, J. W. Kysar, and J. Hone, "Measurement of the elastic properties and intrinsic strength of monolayer graphene," *science*, vol. 321, no. 5887, pp. 385–388, 2008.

[23] V. M. Pereira, A. C. Neto, and N. Peres, "Tight-binding approach to uniaxial strain in graphene," *Physical Review B*, vol. 80, no. 4, p. 045401, 2009.

[24] A. A. Balandin, S. Ghosh, W. Bao, I. Calizo, D. Teweldebrhan, F. Miao, and C. N. Lau, "Superior thermal conductivity of single-layer graphene," *Nano letters*, vol. 8, no. 3, pp. 902–907, 2008.

[25] K. Momma and F. Izumi, "VESTA 3 for three-dimensional visualization of crystal, volumetric and morphology data," *J. Appl. Crystallogr.*, vol. 44, p. 1272–1276, 2011.

[26] A. Kuc, N. Zibouche, and T. Heine, "Influence of quantum confinement on the electronic structure of the transition metal sulfide t s 2," *Physical review B*, vol. 83, no. 24, p. 245213, 2011.

[27] C.-J. Shih, Q. H. Wang, Y. Son, Z. Jin, D. Blankschtein, and M. S. Strano, "Tuning on–off current ratio and field-effect mobility in a mos2–graphene heterostructure via schottky barrier modulation," *ACS nano*, vol. 8, no. 6, pp. 5790–5798, 2014.

[28] J. Schwestka, H. Inani, M. Tripathi, N. McEvoy, F. Libisch, F. Aumayr, J. Kotakoski, and R. Wilhelm, "Atomic-Scale Carving of Nanopores into a van der Waals Heterostructure with Slow Highly Charged Ions," *ACS Nano*, vol. 14, p. 10536, 2020.

[29] R. Wilhelm, *Wechselwirkung langsamer hochgeladener Ionen mit Ionenkristalloberflächen und ultradünnen Kohlenstoffmembrane*. PhD thesis, TU Dresden, 2014.

[30] R. Wilhelm, E. Gruber, R. Ritter, R. Heller, S. Facsko, and F. Aumayr, "Charge exchange and energy loss of slow highly charged ions in 1 nm thick carbon nanomembranes," *Physical review letters*, vol. 112, p. 153201, 04 2014.

[31] R. Wilhelm and P. Grande, "Unraveling energy loss processes of low energy heavy ions in 2d materials," *Communications Physics*, 2019.

[32] G. L. Szabo, B. R. Jany, H. Muckenhuber, A. Niggas, M. Lehner, A. Janas, P. S. Szabo, Z. Gan, A. George, A. Turchanin, *et al.*, "Charge-state-enhanced ion sputtering of metallic gold nanoislands," *Small*, p. 2207263, 2023.

[33] A. Niggas, J. Schwestka, K. Balzer, D. Weichselbaum, N. Schlünzen, R. Heller, S. Creutzburg, H. Inani, M. Tripathi, C. Speckmann, *et al.*, "Ion-induced surface charge dynamics in freestanding monolayers of graphene and mos 2 probed by the emission of electrons," *Physical Review Letters*, vol. 129, no. 8, p. 086802, 2022.

[34] R. Wilhelm, E. Gruber, J. Schwestka, R. Kozubek, T. Madeira, J. Marques, J. Kobus, A. Krasheninnikov, M. Schleberger, and F. Aumayr, "Interatomic Coulombic Decay: The Mechanism for Rapid Deexcitation of Hollow Atoms," *Physical Review Letters*, vol. 119, p. 103401, 2017.

[35] R. Wilhelm, E. Gruber, J. Schwestka, R. Heller, S. Facsko, and F. Aumayr, "Neutralization Dynamics of Slow Highly Charged Ions in 2D Materials," *Applied Sciences*, vol. 8, 2018.

[36] R. A. Wilhelm, "The charge exchange of slow highly charged ions at surfaces unraveled with freestanding 2d materials," *Surface Science Reports*, p. 100577, 2022.

[37] W. Sartison, "New experimental setup to perform light ion transmission through freestanding 2D materialsials," Master's thesis, TU Wien and HAWK Göttingen, 2022.

[38] E. Gruber, *Interaction of ions with 2D and 3D materials*. PhD thesis, TU Wien, 2017.

[39] E. Galutschek, R. Trassl, E. Salzborn, F. Aumayr, and H. Winter, *Compact, low-cost 14.5 GHz all-permanent magnet field ECR multiply charged ion source*. TU Wien.

[40] J. Schwestka, *On the charge exchange dynamics of highly charged ions in atomically thin solids*. PhD thesis, TU Wien, 2020.

[41] Graphenea, "Suspended graphene on tem grids (quantifoil gold) - pack 4 units," *https://www.graphenea.com/collections/graphene-tem-grids/products/suspended-monolayer-graphene-on-tem-grids*, 2022 (accessed on November 18, 2022).

[42] A. Niggas, "The role of contaminations in the interaction of highly charged ions with 2D materials," Master's thesis, TU Wien, 2019.

[43] A. Niggas, J. Schwestka, S. Creutzburg, T. Gupta, D. Eder, B. Bayer, F. Aumayr, and R. Wilhelm, "The role of contaminations in ion beam spectroscopy with freestanding 2d materials: a study on thermal treatment," *The Journal of Chemical Physics*, vol. 153, p. 014702, 2020.

A. Appendix

This brief appendix is targeted at future students working at BeamLine1 and shows the used power supplies, electronic devices and their wiring as well as the assignment of the vacuum feedthroughs on top of the vacuum chamber.

A.1. Electronic rack and wiring

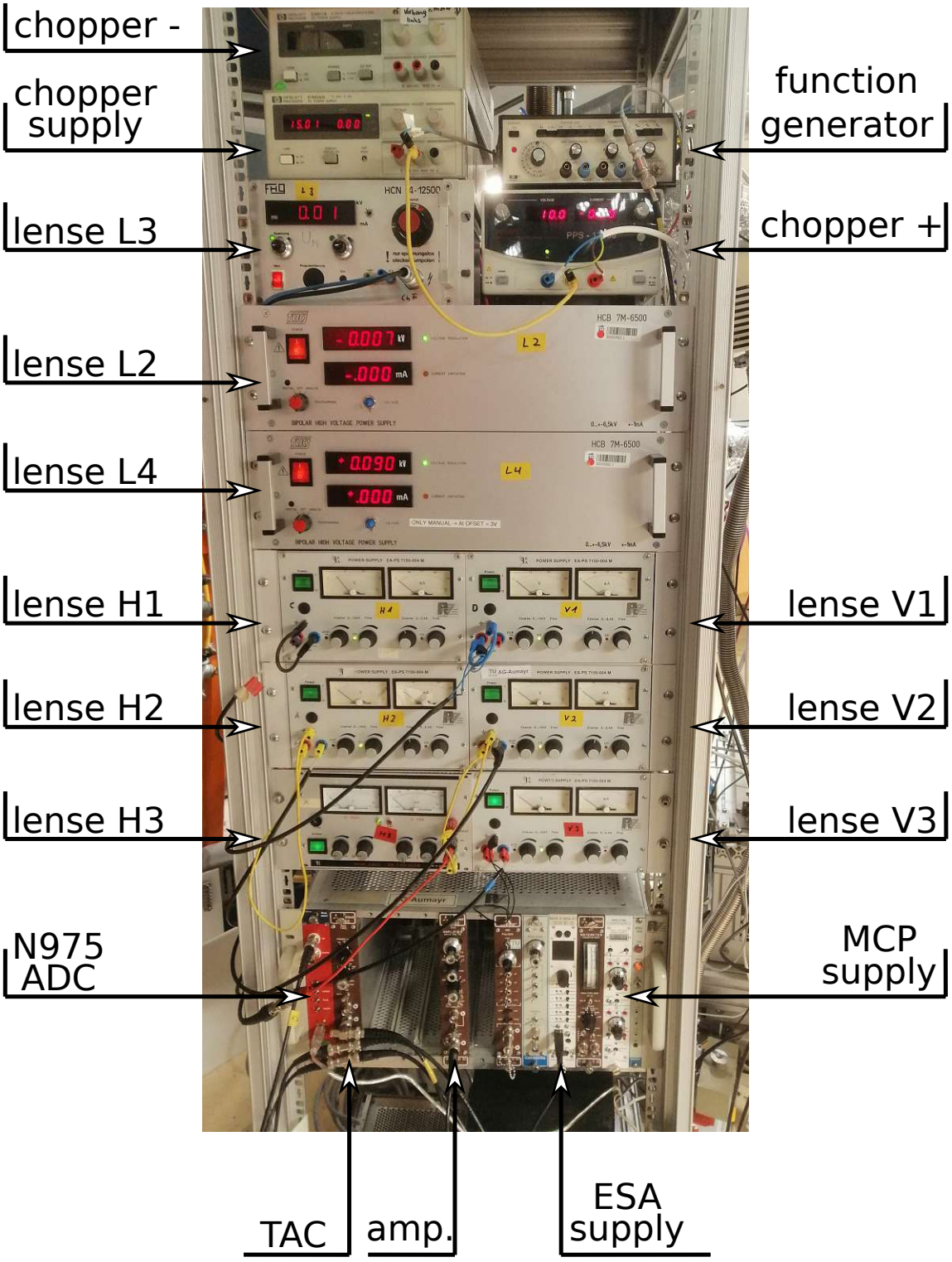

Figure A.1.: Power supplies and TOF electronics.

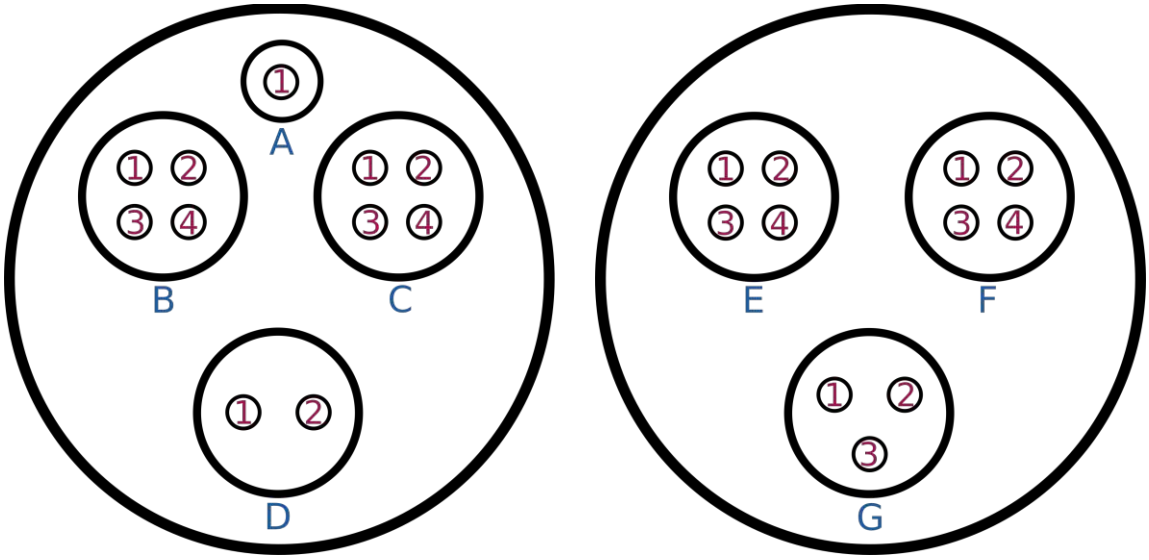

(a) Lens system (b) Detection electronics

Figure A.2.: Feedthrough assignment. (top view, beam direction left to right)

Connector number	Connected with	Connector type
A1	L4 (Einzel lens)	SHV
B1	V3 (deflection plate)	SHV
B2	H3 (deflection plate)	SHV
B3	L3 (Einzel lens)	SHV
B4	L2 (Einzel lens)	SHV
C1	H2 (deflection plate)	MHV
C2	H1 (deflection plate)	MHV
C3	V2 (deflection plate)	MHV
C4	V1 (deflection plate)	MHV
D1	A2 (aperture)	BNC
D2	A3 (aperture)	BNC
E1	ESA+	SHV
E2	ESA-	SHV
E3	MCP1- (HV)	SHV
E4	MCP2- (HV)	SHV
F1	MCP1 Signal	MHV
F2	MCP2 Signal	MHV
F3	MCP1+ (ground)	MHV
F4	MCP1+ (ground)	MHV
G1	ESA L1 (aperture)	MHV
G2	ESA L2 (aperture)	MHV
G2	ESA Side	MHV